Observation of Giant Nernst Plateau in Ideal 1D Weyl Phase

Y. Zhang, 1,2,3,* J. Q. Cai, 1,2,* Peng-Lu Zhao, 4,5,6,*,† Q. Li, 1,2 Y. C. Qian, 1,2 Y. Y. Lv, Y. B. Chen, Q. Niu, 4,7 Hai-Zhou Lu, 6,5,‡ J. L. Zhang, 1,8 and M. L. Tian, Magnetic Field Laboratory, HFIPS, Chinese Academy of Sciences, Hefei 230031, China

2 Science Island Branch, Graduate School of USTC, Hefei 230026, China

3 National Laboratory of Solid State Microstructures, Nanjing University, Nanjing 210093, China

4 Department of Physics, University of Science and Technology of China, Hefei, Anhui 230026, China

5 Quantum Science Center of Guangdong-Hong Kong-Macao Greater Bay Area (Guangdong), Shenzhen 518045, China

6 State Key Laboratory of Quantum Functional Materials, Department of Physics, and

Guangdong Basic Research Center of Excellence for Quantum Science, Southern University of Science and Technology (SUSTech), Shenzhen 518055, China

7 CAS Key Laboratory of Strongly-Coupled Quantum Matter Physics, University of Science and Technology of China, Hefei, Anhui 230026, China

⁸School of Physics and Optoelectronics Engineering, Anhui University, Hefei, Anhui 230601, China

(Received 16 December 2024; revised 27 August 2025; accepted 9 September 2025; published 21 October 2025)

The search for a giant Nernst effect beyond conventional mechanisms offers advantages for developing advanced thermoelectric devices and understanding charge-entropy conversion. Here, we study the Seebeck and Nernst effects in HfTe₅ across a broad range of magnetic fields. Remarkably, the Nernst effect forms a giant plateau at ultrahigh magnetic fields ($B > 10B_{QL}$), with the magnitude reaching up to 50 μ V/K at 2 K. By tracking two magnetic-field-driven phase transitions predicted for weak topological insulators, we find that the giant Nernst plateau exists exclusively in the ideal 1D Weyl phase. Theoretical analysis further demonstrates that such a giant Nernst plateau arises from the unique thermoelectric conversion mechanism inherent to the ideal 1D Weyl phase, where the transverse thermoelectric effect (Nernst effect) is dominated by the longitudinal conduction channel. Our findings expand the understanding of ideal Weyl physics and open new avenues for significantly improving thermoelectric conversion efficiency.

DOI: 10.1103/4zlp-n5qm

Introduction—One of the representative transverse thermoelectric effects is the anomalous Nernst effect (ANE), where S_{xy} initially increases, saturates, and forms a plateau in a range of weak magnetic fields. It has been recognized that the large Berry curvature, originating from Bloch electronic bands with spin-orbit coupling, can generate a significant transverse response [1]. With this strategy, large ANE has been demonstrated in a few topological ferromagnets [2–7] and antiferromagnets [8,9]. Despite these advancements, the transverse thermoelectric effect is typically several orders of magnitude weaker than its longitudinal counterpart. Moreover, it decays drastically with decreasing temperature. The discovery of a new working mechanism that can overcome these limitations is highly desirable.

In analogy to Bloch bands, electrons experience Landau quantization and form the Landau band spectrum under external magnetic fields. The system reaches its quantum limit (B_{OL}) when all electrons in a band are confined to the lowest Landau level. Within this regime, 3D topological materials exhibit a range of exotic quantum phenomena intrinsically associated with their particular band topology, including 3D quantum Hall [10-13], 3D metal to insulator transition [11,12,14], Berry paramagnetism [15-17], and Weyl node annihilation [18,19]. Transition metal pentatellurides ZrTe₅ and HfTe₅ exhibit multiple topological phases [20]. More importantly, their extremely small Fermi surfaces enable the study to be extended deeper into the quantum limit than in other 3D materials. Besides the gap-closing transition at B₁ [Fig. 1(c)], another topological Lifshitz transition B₂ [Fig. 1(d)], proposed for weak topological insulators (see Supplemental Material Sec. SV [21]), was recently observed in HfTe₅ [35,41]. Above B_2 , further increasing the magnetic field drives the Fermi energy toward the 1D Weyl points and eventually forms the ideal 1D Weyl phase above B_3 [Fig. 1(e)]. Such a 1D

These authors have contributed equally to this work.

[†]Contact author: zhaoplu@gmail.com †Contact author: luhz@sustech.edu.cn *Contact author: zhangijnglei@hmfl.ac.cn |Contact author: tianml@hmfl.ac.cn

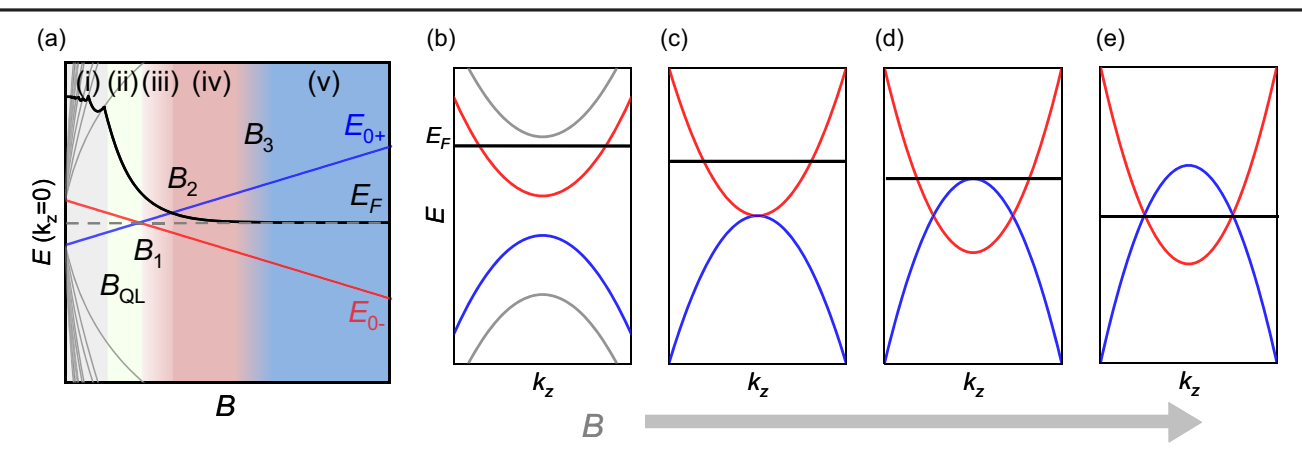


FIG. 1. Sketch of magnetic-field-induced Landau band transitions. (a) Landau bands at $k_z=0$ and Fermi level (E_F) for a 3D weak topological insulator versus the magnetic field. The red, blue, and gray lines represent the zeroth Landau bands E_{0+} (electron), E_{0-} (hole), and high-index Landau bands, respectively. The black line represents the Fermi energy E_F . The (i)–(v) regions represent different phases: (i) the 3D weak topological insulator state, (ii) the system reaches the quantum limit, (iii) the 1D trivial semiconductor state, (iv) the 1D Weyl phase, and (v) the ideal 1D Weyl phase. (b)–(e) Evolution of the Landau bands for weak topological insulators under selected magnetic fields. (b) Fermi level crosses only the zeroth Landau band at the quantum limit $B_{\rm QL}$. (c) Gap of the zeroth Landau band closes at the critical field B_1 . (d) Topological Lifshitz transition occurs at B_2 , where the Fermi level crosses the bottom of E_{0-} . (e) Ideal 1D Weyl phase with all Weyl points located at E_F . B_3 is the critical field at which the Fermi energy approaches sufficiently close to the 1D Weyl points, enabling the observation of quantum transport unique to the ideal 1D Weyl phase.

feature of the Weyl node gives rise to distinct quantum transport compared to that in other dimensions, making it highly suitable for exploring novel thermoelectric conversion mechanisms.

In this Letter, we investigate a new thermoelectric conversion mechanism in the ultrahigh magnetic field where $B>10B_{QL}$. We measure the thermoelectric effects of the high-mobility hafnium pentatelluride (HfTe₅) in magnetic fields up to 33 T. Our results show that, upon the formation of the ideal 1D Weyl phase, the Nernst signal becomes field independent, establishing a plateau with a magnitude that can reach up to $50 \,\mu\text{V/K}$ at 2 K. Furthermore, we theoretically argue that the transverse thermoelectric effect (Nernst effect) in the ideal 1D Weyl phase is dominated by the longitudinal conduction channel, which accounts for the observed giant Nernst plateau in high magnetic fields.

Experimental details—High quality single crystals HfTe₅ were synthesized using the iodine vapor transport method in a two-zone furnace. Figure 2(a) presents the orthorhombic crystal structure of HfTe₅, and we define x, y, and z as directed along a, c, and b, respectively. $-S_{xx}$ and S_{xy} were measured with the DC method in a superconducting magnet (0–9 T) and with the AC method in a water-cooled magnet. Thermoelectric experiments were carried out with the thermal gradient along the a axis and the magnetic field along the b axis [see Fig. 2(b)]. The high-field measurements up to 33 T were performed at the Chinese High Magnetic Field Laboratory at Hefei using a resistive water-cooled magnet. More experimental details are described in Supplemental Material Sec. SII [21].

Gap closing of zeroth Landau bands at B_1 —Hereafter, we present our main results in order of increasing magnetic field, starting from zero. The inset of Fig. 2(c) illustrates the temperature-dependent resistivity with a peak at around $T^* = 65 \text{ K}$, which is a typical feature of transitionpentatelluride samples and is attributed to the shift of the Fermi energy from the valence band toward the conduction band as the temperature decreases [36]. Figures 2(c) and 2(d) display the longitudinal (Seebeck) and transverse (Nernst) thermoelectric responses as functions of magnetic field at selected temperatures. At low temperatures, clear quantum oscillations can be identified in both $-S_{xx}$ and S_{xy} . The fitted quantum limit for S1 is approximately $B_{\rm QL}=1.45$ T. After the system enters the quantum limit, $-S_{xx}$ exhibits a significant drop, with a magnitude surpassing the quantum oscillations observed at lower magnetic fields. In addition to the drastic drop, the Seebeck signal approaches zero at B_1 , while the Nernst signal exhibits a sign reversal. For a nontrivial topological system, band inversion and Zeeman effects drive the two zeroth Landau bands to cross each other at the critical field B_1 [Fig. 1(c)]. The typical transport responses at B_1 have been investigated in ZrTe₅ and Pb_{1-x}Sn_xSe [37,42-44]. Qualitatively, our experimentally resolved profile bears a similar appearance to theirs. However, due to the lower carrier density and smaller gap size, the critical field B_1 of our sample (3.2 T at 2 K) is much lower than that in previous studies. As the gap size is enlarged with increasing temperature, warming the sample shifts B_1 slightly to a higher magnetic field [inset of Fig. 2(d)].

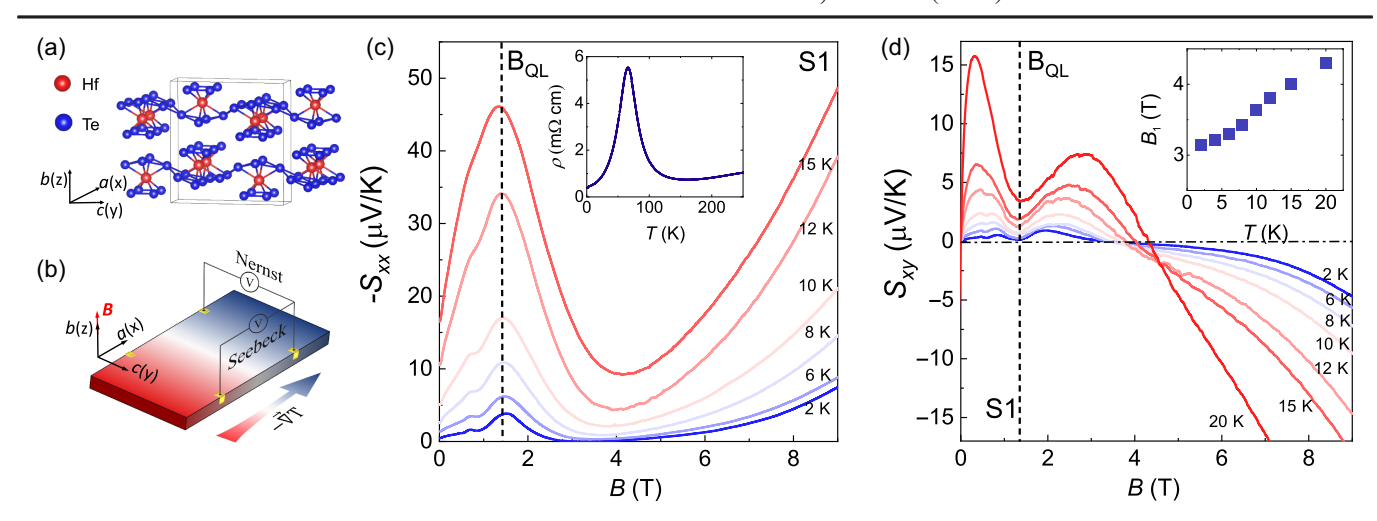


FIG. 2. Unusual thermoelectric response at B_1 . (a) Crystal structure of HfTe₅. (b) Schematic diagram of thermoelectric effect measurements. In a perpendicular magnetic field and a longitudinal thermal gradient, carrier diffusion generates a longitudinal electric field $E_x = -S_{xx}|\nabla T|$ (Seebeck effect) and a transverse electric field $E_y = S_{xy}|\nabla T|$ (Nernst effect). (c),(d) Magnetic field dependence of the thermopower $-S_{xx}$ and Nernst signal S_{xy} at several temperatures below 20 K. The vertical dashed line in both diagrams represents the magnetic field at the quantum limit (B_{QL}). The gap closure in the zeroth Landau band is indicated at B_1 , with $-S_{xx}$ approaching its minimum and S_{xy} undergoing a sign reversal. Inset: (c) Temperature dependence of the electrical resistivity [$\rho(T)$] of HfTe₅ at zero magnetic field. (d) Temperature dependence of B_1 .

Topological Lifshitz transition at B_2 —Figures 3(a) and 3(b) present $-S_{xx}$ and S_{xy} of sample S2, measured with a magnetic field up to 33 T. The low-field behavior closely matches the results of S1. As the magnetic field increases, the thermopower exhibits a continuous rise until reaching its maximum at B = 11 T, after which it decays. This behavior contrasts with theoretical expectations, which suggest that the thermopower of Dirac and Weyl semimetals should grow linearly with the field without saturation [45]. The peak of $-S_{xx}$ in the quantum limit was conjectured to result from a metal-insulator transition, caused by either charge density wave formation or the magnetic freeze-out effect [11,46]. However, this interpretation has been questioned due to the absence of the thermodynamic evidence expected for a charge density wave transition [13]. Moreover, ρ_{xx} bends above 20 T and approaches saturation instead of continuing to diverge as expected for the magnetic freeze-out effect.

As shown in Fig. 1(a), for a weak topological insulator, the dispersive Landau bands would induce a Lifshitz transition at B_2 [Fig. 1(d)]. The main consequence for a Lifshitz transition on transport properties is the change of the scattering rate [38–40]. In our case, the topological change of the FS will act as a trap for electrons in the scattering process from E_{0-} to E_{0+} through impurities. Thus, the peak in $-S_{xx}$ can be regarded as the fingerprint of a topological Lifshitz transition at B_2 . Theoretically, B_2 can be estimated from (see Supplemental Material Sec. SVIII [21])

$$2M_z \left(\frac{\pi h n}{e}\right)^2 - \alpha B_2^3 + \left(\Delta + \frac{\hbar^2 v_z^2}{2M_z}\right) B_2^2 = 0, \quad (1)$$

which indicates that $B_2 \sim n^{2/3}$ and $B_2 \sim v_z^2$. The carrier density of our sample in zero field is approximately $n_0 = 6.0 \times 10^{17}/\text{cm}^3$. By substituting this value into Eq. (1) with $v_z = 0$, the calculated value is approximately 13 T, which is consistent with the experimentally measured B_2 (the peak of $-S_{xx}$).

The temperature dependence of the measured B_2 can also be also qualitatively explained within this scenario. The previous angle-resolved photoemission spectroscopy (ARPES) experiment [36] indicates that, as the temperature increases, the zero-field Fermi level moves closer to the Dirac point, making the contribution of the linear band more significant. As a result, v_z increases with temperature, leading to a temperature-dependent enhancement of B_2 . Taking $v_z(15 \text{ K}) = 6 \times 10^4 \text{ m/s}$ with the same carrier density results in $B_2 \approx 60 \text{ T}$ [Fig. 4(c)], which is beyond the accessible range of our Letter. In the case without such a topological Lifshitz transition, $-S_{xx}$ exhibits saturating behavior, as expected in a trivial semimetal.

Giant Nernst plateau above B_3 —We now present the high-field Nernst plateau shown in Fig. 3(b). Notably, at low temperatures, after an initial decrease, S_{xy} develops an extended plateau beyond a saturation field. The saturating behavior of S_{xy} indicates the presence of an anomalous, i.e., a magnetic-field-independent component in the Nernst signal. Such an anomalous term can reach an ultrahigh value of 50 μ V/K at 2 K. As the temperature increases, the onset of the plateau moves to a higher magnetic field, and its height increases [see Fig. 3(d)], reaching 110 μ V/K at the maximum temperature of 10 K, where the plateau remains clearly visible. Recently, the presence of a nonzero Berry curvature from the spin-split massive Dirac bands has

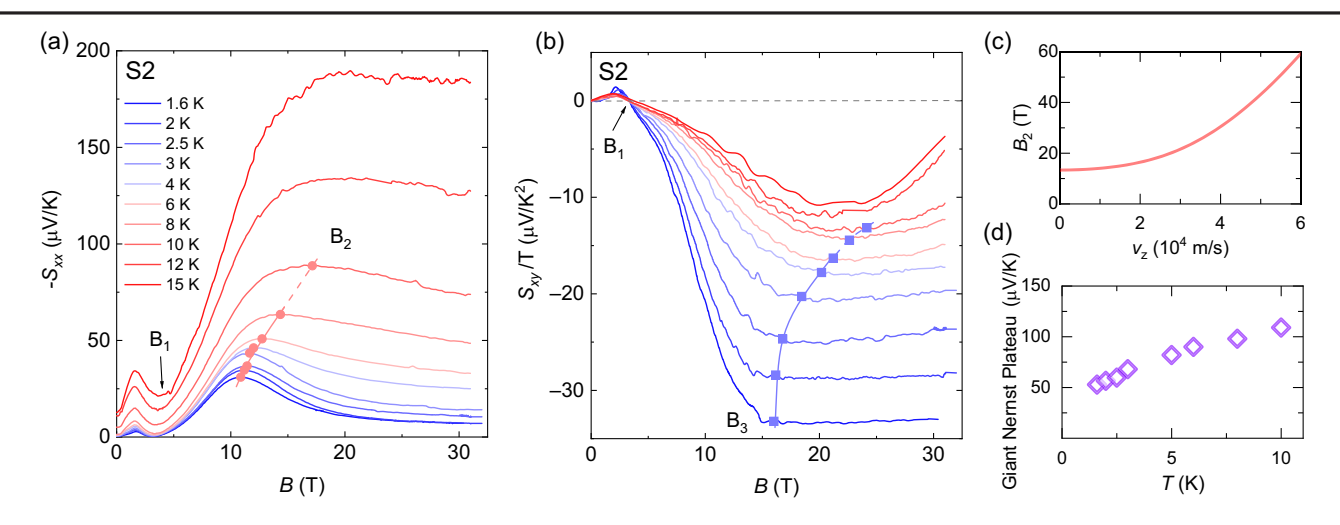


FIG. 3. Giant Nernst plateau in ideal 1D Weyl states. (a) High-field measurements of $-S_{xx}$ up to 33 T at several temperatures. The profiles below 9 T are similar to Fig. 2(d). The critical field B_2 for the topological Lifshitz transition is identified from the maximum of $-S_{xx}$ (marked by red circles). B_2 shifts to higher magnetic fields with increasing temperature and is not observable above 10 K. (b) High-field measurements of the normalized Nernst effect S_{xy}/T at the same temperatures as in (a). A plateau can be observed below 10 K. B_3 is identified by the field where S_{xy}/T starts to saturate (marked by blue squares). (c) Dependence of B_2 on v_z , calculated using Eq. (1), with the following parameters: $M_{\perp} = -12.24 \text{ eV} \cdot \text{Å}^2$, $M_z = 2.7 \text{ eV} \cdot \text{Å}^2$, $n = 6 \times 10^{17}/\text{cm}^3$, g = 12, and $\Delta = 2.5 \text{ meV}$. (d) Summary of the giant Nernst plateau values.

been proposed to explain the high-field anomalous Hall and Nernst effect in nonmagnetic topological materials [46–51]. However, it may not apply in this case because Berry curvature is absent in 1D Landau bands. Because of the compensation between electron carriers and hole carriers from E_{0-} , the carrier density above B_2 would drop significantly. As a result, the higher magnetic fields would immediately push the Fermi energy toward the two 1D Weyl points, forming the ideal Weyl phase. In this sense, the high-field Nernst plateau exclusively above B_2 strongly indicates an intrinsic correlation with the ideal 1D Weyl phase.

We theoretically demonstrate that the observed plateau in S_{xy} is caused by the ideal 1D Weyl phase shown in Fig. 1(e). When $B > B_2$, the change of n cannot be ignored, while E_F varies slightly with the magnetic field (see Supplemental Material Sec. SVIII [21]). Hence the calculation above B_2 is performed with the fixed E_F . According to the Mott relation, $S_{xy} = L_0 e(\rho_{xx} \partial \sigma_{xy} / \partial E_F - \rho_{yx} \partial \sigma_{xx} / \partial E_F)$, where $L_0 = \pi^2 k_B^2 T/3e^2$ denotes the Lorentz number. The conductivity meets the requirements $\sigma_{xy}(-E_F) = -\sigma_{xy}(E_F)$ and $\sigma_{xx}(-E_F) = \sigma_{xx}(E_F)$. Thus, in the ideal 1D Weyl phase where $\partial \sigma_{xx}/\partial E_F|_{E_F\to 0}=0$, the Nernst coefficient is determined by $S_{xy} = L_0 e \sigma_{xx}^{-1} \partial \sigma_{xy} / \partial E_F$, where σ_{xy} contains only the Drude term and the anomalous Hall is not included. Based on the Kubo formula, we obtain $\partial \sigma_{xy}/\partial E_F =$ $-2/(\pi R_{\rm K} v_{\rm w})$ and $\sigma_{xx} = \Gamma/(\pi R_{\rm K} v_{\rm w})$ (see Supplemental Material Sec. SIX [21]), where $R_{\rm K} = h/e^2$ denotes the von Klitzing constant, $v_w = 2\sqrt{M_z(\alpha B - \Delta)}$ denotes the Fermi velocity of the ideal 1D Weyl phase, and Γ is the energy broadening of the Landau bands. As a result,

the Nernst coefficient is given by

$$\frac{S_{xy}}{T} = -\frac{\pi^2 k_B^2}{3e} \frac{2}{\Gamma}.$$
 (2)

Apart from the basic constants $\pi^2 k_B^2/3e$, the Nernst coefficient is entirely determined by the energy broadening parameter Γ , which is field independent in the quantum limit [52–54]. By taking $\Gamma = 2 \text{ meV} \sim \Delta$, the plateau value is obtained as $S_{xy}/T = -24.4 \, \mu V/K^2$, which is comparable to the experimentally measured values. For a higher temperature, a larger Γ is expected [55], and thus a lower S_{xy}/T is achieved. Our complete theory not only explains the origin of the plateau but also predicts the behavior of $S_{xy}(B)$ in the quantum limit, which is in excellent agreement with experimental results, as shown in Fig. 4(a). Moreover, ρ_{xx} = $\sigma_{xx}^{-1} = (\pi R_K v_w)/\Gamma$ in the ideal 1D Weyl phase suggests that ρ_{xx} increases with the magnetic field as $\sqrt{aB} - b$. The measured magnetoresistance $\{[\rho_{xx}(B) - \rho_{xx}(0)]/\rho_{xx}(0)\}$ shown in Fig. 4(b) can be well fitted by this expression when B > 15 T (ideal 1D Weyl phase), which further confirms the validity of our explanations.

Discussions—We summarize our findings with a phase diagram in the B-T plane, shown in Fig. 4(c). Phenomenally, the giant Nernst plateau observed here is quite similar to the widely reported ANE [1]. However, they differ fundamentally in both experimental measurements and theoretical interpretations. First, the giant Nernst plateau occurs at an ultrahigh magnetic field ($B > 10B_{QL}$), while ANE is a low-field effect. To our knowledge, no experiments have observed plateaus in such strong magnetic fields. Second, the giant Nernst plateau represents the

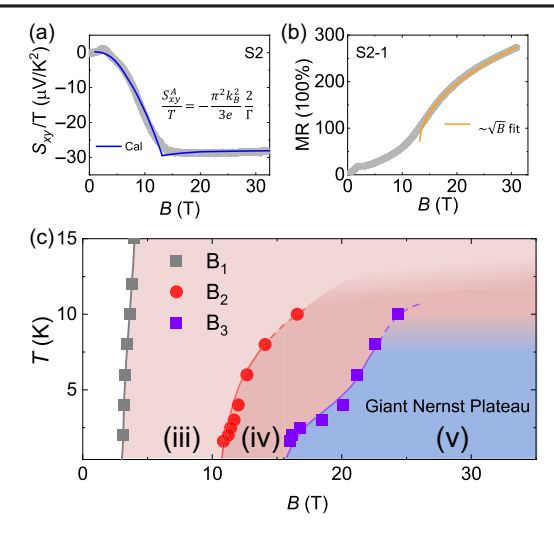


FIG. 4. Comparisons of experimental measurements and theoretical calculations. (a) Experimental (gray line) and calculated S_{xy}/T (blue) at 2 K. S_{xy}/T is calculated by fixing n as a constant before the Lifshitz transition (\approx 13 T) and fixing $E_F=0$ after the Lifshitz transition (see Supplemental Material Sec. SVIII for details [21]), with the following parameters: $M_{\perp}=-12.24~{\rm eV}\cdot {\rm Å}^2,~M_z=2.7~{\rm eV}\cdot {\rm Å}^2,~n=8.8\times 10^{16}/{\rm cm}^3,~g=12,$ and $\Delta=2.5~{\rm meV}$. (b) Magnetoresistance of HfTe₅ measured at 2 K. The yellow line represents a fit with $\sqrt{aB-b}$, where a and b are constants. (c) Temperature-magnetic field phase diagram of HfTe₅. The values of B_1 , B_2 , and B_3 are transferred from Fig. 3, and (iii)–(v) denote the corresponding phases in Fig. 1(a).

new mechanism of thermoelectric conversion, where the plateau is quite different from the semiclassical theories for ANE [1]. Notably, such a plateau is unrelated to the anomalous Hall conductivity since our theoretical calculations show that the Hall conductivity contains only the Drude term after the formation of Landau bands (Supplemental Material Sec. SVII [21]). Finally, the giant Nernst plateau (S_{xy}/T) is exceptionally large, surpassing any measured ANEs to date [2-9,47-49], and Eq. (2) indicates that increasing mobility can further enhance its magnitude. Moreover, reducing the carrier density will significantly lower the magnetic field required to form the ideal 1D Weyl phase. In this sense, the weak topological insulators with extremely low quantum limit have potential applications in the development of novel thermoelectric devices.

Acknowledgments—We acknowledge very helpful discussions with X. Yuan, C. L. Zhang, C. Zhang, and Z. J. Xiang. This work was financially supported by the National Key R&D Program of the MOST of China (Grants No. 2022YFA1602602, No. 2022YFA1602603, No. 2022YFA1403700, and No. 2023YFA1406300), the National Natural Science Foundation of China (Grants No. 12474053, No. 12525401, No. 12122411, No. 12304074, No. 12234017, No. 12374041, and No. 12350402), the Basic

Research Program of the Chinese Academy of Sciences Based on Major Scientific Infrastructures (Grant No. JZHKYPT-2021-08), Guangdong Basic and Applied Basic Research Foundation (Grant No. 2023B0303000011), Guangdong Provincial Quantum Science Strategic Initiative (Grants No. GDZX2201001 and No. GDZX2401001), the Science, Technology and Innovation Commission of Shenzhen Municipality (Grant No. ZDSYS20190902092905285), High-level Special Funds (G03050K004), and the New Cornerstone Science Foundation through the XPLORER PRIZE. We thank the WM5 ([56]) at the Steady High Magnetic Field Facility, CAS ([57]), for providing technical support and assistance in data collection and analysis. The numerical calculations were supported by the Center for Computational Science and Engineering of SUSTech.

Data availability—The data that support the findings of this article are not publicly available upon publication because it is not technically feasible and/or the cost of preparing, depositing, and hosting the data would be prohibitive within the terms of this research project. The data are available from the authors upon reasonable request.

- N. Nagaosa, J. Sinova, S. Onoda, A. H. MacDonald, and N. P. Ong, Anomalous Hall effect, Rev. Mod. Phys. 82, 1539 (2010).
- [2] A. Sakai, Y. P. Mizuta, A. A. Nugroho, R. Sihombing, T. Koretsune, M.-T. Suzuki *et al.*, Giant anomalous Nernst effect and quantum-critical scaling in a ferromagnetic semimetal, Nat. Phys. **14**, 1119 (2018).
- [3] L. Ye, M. Kang, J. Liu, F. Von Cube, C. R. Wicker, T. Suzuki *et al.*, Massive Dirac fermions in a ferromagnetic kagome metal, Nature (London) 555, 638 (2018).
- [4] S. N. Guin, P. Vir, Y. Zhang, N. Kumar, S. J. Watzman, C. Fu *et al.*, Zero-field Nernst effect in a ferromagnetic kagome-lattice Weyl-semimetal Co₃Sn₂S₂, Adv. Mater. 31, 1806622 (2019).
- [5] H. Yang, W. You, J. Wang, J. Huang, C. Xi, X. Xu *et al.*, Giant anomalous Nernst effect in the magnetic Weyl semimetal Co₃Sn₂S₂, Phys. Rev. Mater. **4**, 024202 (2020).
- [6] T. Asaba, V. Ivanov, S. M. Thomas, S. Y. Savrasov, J. D. Thompson, E. D. Bauer, and F. Ronning, Colossal anomalous Nernst effect in a correlated noncentrosymmetric kagome ferromagnet, Sci. Adv. 7, abf1467 (2021).
- [7] T. Chen, S. Minami, A. Sakai, Y. Wang, Z. Feng, T. Nomoto et al., Large anomalous Nernst effect and nodal plane in an iron-based kagome ferromagnet, Sci. Adv. 8, abk1480 (2022).
- [8] M. Ikhlas, T. Tomita, T. Koretsune, M. T. Suzuki, D. Nishio-Hamane, R. Arita, Y. Otani, and S. Nakatsuji, Large anomalous Nernst effect at room temperature in a chiral antiferromagnet, Nat. Phys. 13, 1085 (2017).
- [9] Y. Pan, C. Le, B. He, S. J. Watzman, M. Yao, J. Gooth, J. P. Heremans, Y. Sun, and C. Felser, Giant anomalous Nernst signal in the antiferromagnet YbMnBi₂, Nat. Mater. 21, 01149 (2022).

- [10] C. Zhang, Y. Zhang, X. Yuan, S. Lu, J. Zhang, A. Narayan *et al.*, Quantum Hall effect based on Weyl orbits in Cd₃As₂, Nature (London) **565**, 331 (2019).
- [11] F. Tang, Y. Ren, P. Wang, R. Zhong, J. Schneeloch, S. A. Yang *et al.*, Three-dimensional quantum Hall effect and metal-insulator transition in ZrTe₅, Nature (London) **569**, 537 (2019).
- [12] P. Wang, Y. Ren, F. Tang, P. Wang, T. Hou, H. Zeng, L. Zhang, and Z. Qiao, Approaching three-dimensional quantum Hall effect in bulk HfTe₅, Phys. Rev. B 101, 161201(R) (2020).
- [13] S. Galeski, T. Ehmcke, R. Wawrzyńczak, P. M. Lozano, K. Cho, A. Sharma *et al.*, Origin of the quasi-quantized Hall effect in ZrTe₅, Nat. Commun. **12**, 3197 (2021).
- [14] P. Wang, F. Tang, P. Wang, H. Zhu, C.-W. Cho, J. Wang, X. Du, Y. Shao, and L. Zhang, Quantum transport properties of β-Bi₄I₄ near and well beyond the extreme quantum limit, Phys. Rev. B 103, 155201 (2021).
- [15] P. J. Moll, A. C. Potter, N. L. Nair, B. J. Ramshaw, K. A. Modic, S. Riggs *et al.*, Magnetic torque anomaly in the quantum limit of Weyl semimetals, Nat. Commun. 7, 12492 (2016).
- [16] C.-L. Zhang, C. M. Wang, Z. Yuan, X. Xu, G. Wang, C.-C. Lee *et al.*, Non-saturating quantum magnetization in Weyl semimetal TaAs, Nat. Commun. 10, 1028 (2019).
- [17] T. Cichorek, Ł. Bochenek, J. Juraszek, Y. V. Sharlai, and G. P. Mikitik, Detection of relativistic fermions in Weyl semimetal TaAs by magnetostriction measurements, Nat. Commun. 13, 3868 (2022).
- [18] C. L. Zhang, S. Y. Xu, C. M. Wang, Z. Lin, Z. Z. Du, C. Guo *et al.*, Magnetic-tunnelling-induced Weyl node annihilation in TaP, Nat. Phys. **13**, 979 (2017).
- [19] B. J. Ramshaw, K. A. Modic, A. Shekhter, Y. Zhang, E. A. Kim, P. J. Moll *et al.*, Quantum limit transport and destruction of the Weyl nodes in TaAs, Nat. Commun. 9, 2217 (2018).
- [20] H. Weng, X. Dai, and Z. Fang, Transition-metal pentatelluride ZrTe₅ and HfTe₅: A paradigm for large-gap quantum spin Hall insulators, Phys. Rev. X 4, 011002 (2014).
- [21] See Supplemental Material at http://link.aps.org/supplemental/ 10.1103/4zlp-n5qm, which includes Refs. [16,22–40], for the experimental methods, analysis of carrier density and mobility, high-field studies of ρ_{xx} and ρ_{xy} , and theoretical calculations.
- [22] R. Y. Chen, Z. G. Chen, X.-Y. Song, J. A. Schneeloch, G. D. Gu, F. Wang, and N. L. Wang, Magnetoinfrared spectroscopy of Landau levels and Zeeman splitting of three-dimensional massless Dirac fermions in ZrTe₅, Phys. Rev. Lett. 115, 176404 (2015).
- [23] Y. Jiang, J. Wang, T. Zhao, Z. L. Dun, Q. Huang, X. S. Wu et al., Unraveling the topological phase of ZrTe₅ via magnetoinfrared spectroscopy, Phys. Rev. Lett. 125, 046403 (2020).
- [24] H. Zhang, C.-X. Liu, X.-L. Qi, X. Dai, Z. Fang, and S.-C. Zhang, Topological insulators in Bi₂Se₃, Bi₂Te₃ and Sb₂Te₃ with a single Dirac cone on the surface, Nat. Phys. 5, 438 (2009).
- [25] E. Martino, I. Crassee, G. Eguchi, D. Santos-Cottin, R. D. Zhong, G. D. Gu *et al.*, Two-dimensional conical dispersion in ZrTe₅ evidenced by optical spectroscopy, Phys. Rev. Lett. **122**, 217402 (2019).

- [26] B. Yan, L. Müchler, and C. Felser, Prediction of weak topological insulators in layered semiconductors, Phys. Rev. Lett. **109**, 116406 (2012).
- [27] A. Abrikosov, Fundamentals of the Theory of Metals (North-Holland, Amsterdam, 1988), Chap. 6.
- [28] A. A. Abrikosov, Quantum magnetoresistance, Phys. Rev. B 58, 2788 (1998).
- [29] H.-Z. Lu, S.-B. Zhang, and S.-Q. Shen, High-field magnetoconductivity of topological semimetals with short-range potential, Phys. Rev. B 92, 045203 (2015).
- [30] H.-Z. Lu and S.-Q. Shen, Weak antilocalization and localization in disordered and interacting Weyl semimetals, Phys. Rev. B 92, 035203 (2015).
- [31] N. Mott and E. Davis, Electronic Processes in Non-Crystalline Materials (Oxford University Press, Oxford, 2012).
- [32] M. Jonson and G. D. Mahan, Mott's formula for the thermopower and the Wiedemann-Franz law, Phys. Rev. B 21, 4223 (1980).
- [33] M. Jonson and S. M. Girvin, Thermoelectric effect in a weakly disordered inversion layer subject to a quantizing magnetic field, Phys. Rev. B 29, 1939 (1984).
- [34] G. D. Mahan, Many Particle Physics, 3rd ed. (Plenum, New York, 2000).
- [35] W. Wu, Z. Shi, Y. Du, Y. Wang, F. Qin, X. Meng *et al.*, Topological Lifshitz transition and one-dimensional Weyl mode in HfTe₅, Nat. Mater. **22**, 84 (2023).
- [36] Y. Zhang, C. Wang, L. Yu, G. Liu, A. Liang, J. Huang et al., Electronic evidence of temperature-induced Lifshitz transition and topological nature in ZrTe₅, Nat. Commun. 8, 15512 (2017).
- [37] J. L. Zhang, C. M. Wang, C. Y. Guo, X. D. Zhu, Y. Zhang, J. Y. Yang *et al.*, Anomalous thermoelectric effects of ZrTe₅ in and beyond the quantum limit, Phys. Rev. Lett. **123**, 196602 (2019).
- [38] A. A. Varlamov and A. V. Pantsulaya, Anomalous kinetic properties of metals near the Lifshitz topological transition, Zh. Eksp. Teor. Fiz. **89**, 2188 (1985), http://www.jetp.ras.ru/cgi-bin/e/index/e/62/6/p1263?a=list.
- [39] Y. M. Blanter, M. I. Kaganov, A. V. Pantsulaya, and A. A. Varlamov, The theory of electronic topological transitions, Phys. Rep. 245, 159 (1994).
- [40] A. A. Varlamov, V. S. Egorov, and A. V. Pantsulaya, Kinetic properties of metals near electronic topological transitions (2 1/2-order transitions), Adv. Phys. **38**, 469 (1989).
- [41] S. Galeski, H. F. Legg, R. Wawrzyńczak, T. Förster, S. Zherlitsyn, D. Gorbunov *et al.*, Signatures of a magnetic-field-induced Lifshitz transition in the ultra-quantum limit of the topological semimetal ZrTe₅, Nat. Commun. 13, 7418 (2022).
- [42] T. Liang, Q. Gibson, J. Xiong, M. Hirschberger, S. P. Koduvayur, R. J. Cava, and N. P. Ong, Evidence for massive bulk Dirac fermions in Pb_{1-x}Sn_xSe from Nernst and thermopower experiments, Nat. Commun. 4, 2696 (2013).
- [43] Y. Liu, X. Yuan, C. Zhang, Z. Jin, A. Narayan, C. Luo *et al.*, Zeeman splitting and dynamical mass generation in Dirac semimetal ZrTe₅, Nat. Commun. 7, 12516 (2016).
- [44] B. A. Assaf, T. Phuphachong, E. Kampert, V. V. Volobuev, P. S. Mandal, J. Sánchez-Barriga *et al.*, Negative

- longitudinal magnetoresistance from the anomalous N=0 Landau level in topological materials, Phys. Rev. Lett. **119**, 106602 (2017).
- [45] B. Skinner and L. Fu, Large, nonsaturating thermopower in a quantizing magnetic field, Sci. Adv. 4, aat2621 (2018).
- [46] A. Gourgout, M. Leroux, J. L. Smirr, M. Massoudzadegan, R. P. Lobo, D. Vignolles *et al.*, Magnetic freeze-out and anomalous Hall effect in ZrTe₅, npj Quantum Mater. 7, 71 (2022).
- [47] T. Liang, J. Lin, Q. Gibson, T. Gao, M. Hirschberger, M. Liu, R. J. Cava, and N. P. Ong, Anomalous Nernst effect in the Dirac semimetal Cd₃As₂, Phys. Rev. Lett. 118, 136601 (2017).
- [48] F. Caglieris, C. Wuttke, S. Sykora, V. Süss, C. Shekhar, C. Felser, B. Büchner, and C. Hess, Anomalous Nernst effect and field-induced Lifshitz transition in the Weyl semimetals TaP and TaAs, Phys. Rev. B 98, 201107(R) (2018).
- [49] S. J. Watzman, T. M. McCormick, C. Shekhar, S. C. Wu, Y. Sun, A. Prakash, C. Felser, N. Trivedi, and J. P. Heremans, Dirac dispersion generates unusually large Nernst effect in Weyl semimetals, Phys. Rev. B 97, 161404(R) (2018).

- [50] Y. Liu, H. Wang, H. Fu, J. Ge, Y. Li, C. Xi *et al.*, Induced anomalous Hall effect of massive Dirac fermions in ZrTe₅ and HfTe₅ thin flakes, Phys. Rev. B **103**, L201110 (2021).
- [51] Z. Sun, Z. Cao, J. Cui, C. Zhu, D. Ma, H. Wang *et al.*, Large Zeeman splitting induced anomalous Hall effect in ZrTe₅, npj Quantum Mater. **5**, 36 (2020).
- [52] E. Gornik, R. Lassnig, G. Strasser, H. L. Störmer, A. C. Gossard, and W. Wiegmann, Specific heat of two-dimensional electrons in GaAs-GaAlAs multilayers, Phys. Rev. Lett. 54, 1820 (1985).
- [53] T. P. Smith, B. B. Goldberg, P. J. Stiles, and M. Heiblum, Direct measurement of the density of states of a two-dimensional electron gas, Phys. Rev. B 32, 2696 (1985).
- [54] R. Ashoori and R. Silsbee, The Landau level density of states as a function of Fermi energy in the two dimensional electron gas, Solid State Commun. **81**, 821 (1992).
- [55] H. P. Wei, A. M. Chang, D. C. Tsui, and M. Razeghi, Temperature dependence of the quantized Hall effect, Phys. Rev. B 32, 7016 (1985).
- [56] https://cstr.cn/31125.02.SHMFF.WM5
- [57] https://cstr.cn/31125.02.SHMFF